

Three-Body Unitary Coupled-Channel Analysis on $\eta(1405/1475)$

S.X. Nakamura,^{1,2,*} Q. Huang,³ J.-J. Wu,^{4,†} H.P. Peng,^{1,2} Y. Zhang,^{1,2} and Y.C. Zhu^{1,2}

¹University of Science and Technology of China, Hefei 230026, China

²State Key Laboratory of Particle Detection and Electronics (IHEP-USTC), Hefei 230036, China

³Department of Physics, Nanjing Normal University, Nanjing, Jiangsu 210097, China

⁴School of Physical Sciences, University of Chinese Academy of Sciences (UCAS), Beijing 100049, China

The recent BESIII data on $J/\psi \rightarrow \gamma(K_S K_S \pi^0)$, which is significantly more precise than earlier $\eta(1405/1475)$ -related data, enables quantitative discussions on $\eta(1405/1475)$ at the previously unreachable level. We conduct a three-body unitary coupled-channel analysis of experimental Monte-Carlo outputs for radiative J/ψ decays via $\eta(1405/1475)$: $K_S K_S \pi^0$ Dalitz plot distributions from the BESIII, and branching ratios of $\gamma(\eta\pi^+\pi^-)$ and $\gamma(\gamma\pi^+\pi^-)$ final states relative to that of $\gamma(K\bar{K}\pi)$. The analysis clarifies $\eta(1405/1475) \rightarrow K\bar{K}\pi$ decay mechanisms, and clearly requires two bare $\eta(1405/1475)$ states in our model. The lower bare state would correspond to a radially excited η' , while the higher one could be an excited $\eta^{(')}$, hybrid, glueball, or a mixture of those. For the three-body unitarity, our model systematically considers (multi-)loop diagrams and an associated triangle singularity, which is critical in making excellent predictions on $\eta(1405/1475) \rightarrow \pi\pi\pi$ lineshapes and branching ratios. The $\eta(1405/1475) \rightarrow \eta\pi\pi$ lineshape is also well predicted. The analysis reveals the $\eta(1405/1475)$ pole locations for the first time. We find two poles for $\eta(1405)$ on different Riemann sheets of the $K^*\bar{K}$ channel, and one pole for $\eta(1475)$.

Introduction.— The nature of isoscalar pseudoscalar meson(s) in 1.4–1.5 GeV region, $\eta(1405/1475)$, has been controversial. On the experimental side, two different states seem to work for $K\bar{K}\pi$ final states produced in π^-p scattering [1, 2], $p\bar{p}$ annihilations [3], and radiative J/ψ decays [4, 5]. However, only one resonant peak, whose position is somewhat process-dependent, is observed in: $\eta\pi\pi$ final states in $p\bar{p}$ annihilation [6] and J/ψ decays accompanied by γ [7–9] and ω [10]; $K\bar{K}\pi$ and $\eta\pi\pi$ final states in $\gamma\gamma$ collisions [11]; $\gamma\rho^0$ final states in radiative J/ψ decays [9, 12, 13] and $p\bar{p}$ annihilation [6]. These data are statistically limited, allowing various theoretical descriptions. In particular, whether $\eta(1405/1475)$ is one or two states remains as a major puzzle.

The quark model predicts only one state, a radially excited $\eta'(958)$, in this energy region and the ideal mixing ($s\bar{s}$) [14, 15] seems consistent with a lattice QCD (LQCD) [16]. To accommodate two states, $\eta(1405)$ was proposed to be a glueball [17], which however is disfavored by LQCD predicting a significantly heavier mass [18–22]. The $\eta(1405/1475)$ couples to quasi two-body channels such as $K^*\bar{K}$ and $a_0\pi$ that further decay to three-body channels such as $K\bar{K}\pi$ and $\pi\pi\eta$, forming a complicated coupled-channel system. Also, a kinematical triangle singularity is caused by the coupled-channel dynamics and plays an important role [23–26]. Thus, a sophisticated coupled-channel analysis of high quality data has been long-awaited to pin down the nature of $\eta(1405/1475)$.

The recent high-statistics BESIII experiment provides a precious opportunity to improve our understanding of $\eta(1405/1475)$. They collected $\sim 10^{10} J/\psi$ decay samples, and conducted an amplitude analysis on $J/\psi \rightarrow \gamma(K_S K_S \pi^0)$ [27]. Their bin-by-bin analysis of the $K_S K_S \pi^0$ invariant mass extracted a $J^{PC} = 0^{-+}$ contri-

bution. Then, their energy-dependent analysis identified two $\eta(1405/1475)$ states with a high statistical significance, and determined their Breit-Wigner (BW) masses and widths. However, the BW amplitude does not respect the unitarity and is therefore not suitable in situations where more than one resonances are overlapping and/or a resonance is close to its decay channel threshold [28]; the situations apply to $\eta(1405)$ and $\eta(1475)$ that are overlapping, and $\eta(1405)$ being close to the $K^*\bar{K}$ threshold. Thus, an important issue is to determine the $\eta(1405/1475)$ pole locations, which can be achieved by analytically continuing a unitary coupled-channel J/ψ decay amplitude fitted to the BESIII data.

Another puzzling issue is a large isospin-violation in $\eta(1405/1475) \rightarrow \pi\pi\pi$ [29]. An explanation has been proposed in Refs. [23–25]: the $K^*\bar{K}K$ -loop mechanism involving a triangle singularity causes the large isospin-violation due to the mass difference between K^\pm and K^0 . Now the issue is to confirm this explanation by examining whether the three-body unitary coupled-channel model fitted to the recent BESIII data [27] can also consistently describe lineshapes and branchings of the three-pion final states; the triangle singularity mechanism is automatically included in the unitary framework.

In this Letter ¹, we conduct a coupled-channel analysis of radiative J/ψ decays via $\eta(1405/1475)$. Our three-body unitary coupled-channel model is fitted to $K_S K_S \pi^0$ Dalitz plot distributions from the BESIII Monte-Carlo (MC) simulation [27], as well as to branching fractions of $\eta\pi^+\pi^-$ and $\rho^0\gamma$ relative to that of $K\bar{K}\pi$. The model will clarify main $\eta(1405/1475)$ decay mechanisms and predict $\eta(1405/1475) \rightarrow \eta\pi\pi, \pi\pi\pi$ lineshapes and branch-

¹ A fuller account of this work will be given separately [30]

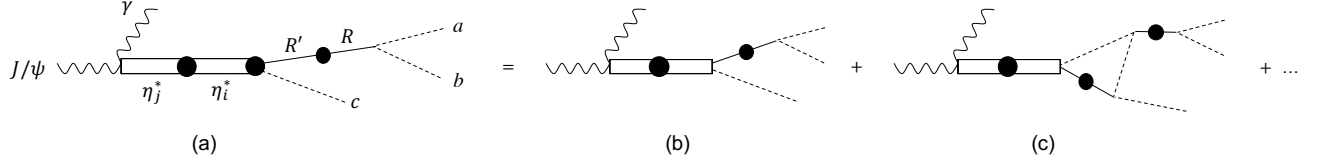


FIG. 1. (a) Radiative J/ψ decay model. The dashed lines represent pseudoscalar mesons while the solid lines are bare two-meson resonances R . The double lines with $\eta_{i(j)}^*$ represent bare states for $\eta(1405)$ and $\eta(1475)$. Dressed propagators and vertices are represented by the solid circles. Main η^* decay mechanisms included in (a) are (b) direct decays and (c) single triangle mechanisms.

ings. The analysis leads to answering three major puzzles regarding $\eta(1405/1475)$:

- Process-dependent lineshapes of $\eta(1405/1475)$ decays
- Large isospin-violation in $\eta(1405/1475) \rightarrow \pi\pi\pi$
- One or two states of $\eta(1405/1475)$, equivalently, pole structure

Model.— A radiative J/ψ decay amplitude² via $\eta(1405/1475)$ excitations is, within our coupled-channel model, diagrammatically represented by Fig. 1(a) and is given by

$$A_{\gamma abc, J/\psi} = \sum_{abc}^{\text{cyclic}} \sum_{RR'} \sum_{s_R^z} \Gamma_{ab, R} \tau_{R, R'}(p_c, E - E_c) \times \bar{\Gamma}_{cR', \eta_i^*}(\mathbf{p}_c, E) \bar{G}_{ij}(E) \Gamma_{\gamma \eta_j^*, J/\psi}, \quad (1)$$

where a , b , and c are pseudoscalar mesons (π , K , η), and R denotes a two-meson resonance such as K^* , κ^3 , $a_0(980)$, and $f_0(980)$; cyclic permutations (abc) , (cab) , (bca) are indicated by $\sum_{abc}^{\text{cyclic}}$; the indices i and j specify one of bare η^* states; E denotes the abc total energy in the abc center-of-mass (CM) frame. The symbols $\Gamma_{\gamma \eta_j^*, J/\psi}$, \bar{G}_{ij} , $\bar{\Gamma}_{cR', \eta_i^*}$, $\tau_{R, R'}$, and $\Gamma_{ab, R}$ denote a $J/\psi \rightarrow \gamma \eta_i^*$ vertex, a dressed η^* propagator, a dressed $\eta_i^* \rightarrow Rc$ decay vertex, a dressed R propagator, and a $R \rightarrow ab$ vertex, respectively, as described below.

The dressed R propagator matrix is given by

$$[\tau^{-1}(p, E)]_{R, R'} = [E - E_R(p)]\delta_{R, R'} - [\Sigma(p, E)]_{R, R'} \quad (2)$$

where a matrix $\Sigma_{R, R'}$ is the R self-energy caused by $\Gamma_{ab, R}$. The dressed $\eta_i^* \rightarrow Rc$ decay vertices $\bar{\Gamma}_{cR', \eta_i^*}$ are

$$\bar{\Gamma}_{cR', \eta_i^*}(\mathbf{p}_c, E) = \int d^3q \Phi_{cR', c'R'}(\mathbf{p}_c, \mathbf{q}; E) \Gamma_{c'R', \eta_i^*}(\mathbf{q}), \quad (3)$$

with $\sum_{c'R's_{R'}^z}$ being implicit; $\Phi = (1 - \int d^3q V\tau)^{-1}$ is a wave function; Γ_{cR, η_i^*} is a bare $\eta_i^* \rightarrow Rc$ decay vertex. The $Rc \rightarrow R'c'$ interaction V includes Z -diagrams in which a $R \rightarrow c'\bar{c}$ is followed by a $\bar{c}c \rightarrow R'$ via a \bar{c} -exchange. An isospin-violating $K^*\bar{K} \rightarrow f_0\pi$ process is caused by a K -exchange Z -diagram and $m_{K^\pm} \neq m_{K^0}$. Formulas for the Z -diagrams can be found in Appendix C of Ref. [31]. The interaction V also includes vector-meson exchange mechanisms, based on the hidden local symmetry model [32], for $K^*\bar{K} \leftrightarrow K^*\bar{K}$, \bar{K}^*K ; see Appendix A of Ref. [33] for formulas. The nonperturbative treatment of $V\tau$ in Eq. (3) is a requirement from the three-body unitarity.

The dressed η^* propagator is given by

$$[\bar{G}^{-1}(E)]_{ij} = (E - m_{\eta_i^*})\delta_{ij} - [\Sigma_{\eta^*}(E)]_{ij}, \quad (4)$$

where $m_{\eta_i^*}$ is the bare mass and the η^* self energy in the second term is

$$[\Sigma_{\eta^*}(E)]_{ij} = \sum_{cRR's_R^z} \int d^3q \Gamma_{cR, \eta_i^*}(\mathbf{q}) \times \tau_{R, R'}(q, E - E_c(q)) \bar{\Gamma}_{cR', \eta_j^*}(\mathbf{q}, E). \quad (5)$$

The default coupled-channels included in our model are two bare η^* states and $Rc = K^*(892)\bar{K}$, $\kappa\bar{K}$, $a_0(980)\pi$, $a_2(1320)\pi$, $f_0\eta$, $\rho(770)\rho(770)$, and $f_0\pi$ ⁴: $\bar{K}^*(892)K$ and $\bar{\kappa}K$ are implicitly included to form positive C -parity states. The bare R states and their decay channels (two-meson continuum states) couple nonperturbatively to generate scattering amplitudes and resonance poles. Thus we can fix the coupling and cutoff parameters in $\Gamma_{ab, R}$ and m_R (bare mass) by fitting $ab \rightarrow ab$ scattering data. Meanwhile, the parameters in Γ_{cR, η_i^*} , $\Gamma_{\gamma \eta_j^*, J/\psi}$, and $m_{\eta_i^*}$ are fitted to MC outputs for $J/\psi \rightarrow \gamma \eta(1405/1475) \rightarrow \gamma(abc)$. To describe the $\gamma(\pi^+\pi^-\gamma)$ final state, we assume the vector-meson dominance mechanism where the $\rho\rho$ channel from the dressed $\eta_i^* \rightarrow \rho\rho$ is followed by $\rho \rightarrow \gamma$ and $\rho \rightarrow \pi^+\pi^-$; no additional parameters.

² We denote a particle x 's mass, momentum, energy, polarization, spin and its z -component in the abc center-of-mass frame by m_x , \mathbf{p}_x , E_x , s_x , and s_x^z , respectively; $E_x = \sqrt{m_x^2 + |\mathbf{p}_x|^2}$. The mass values are from Ref. [14].

³ κ is also referred to as $K_0^*(700)$.

⁴ The $\rho\rho$ channel needs slight modifications of the presented formulas; see Ref. [30].

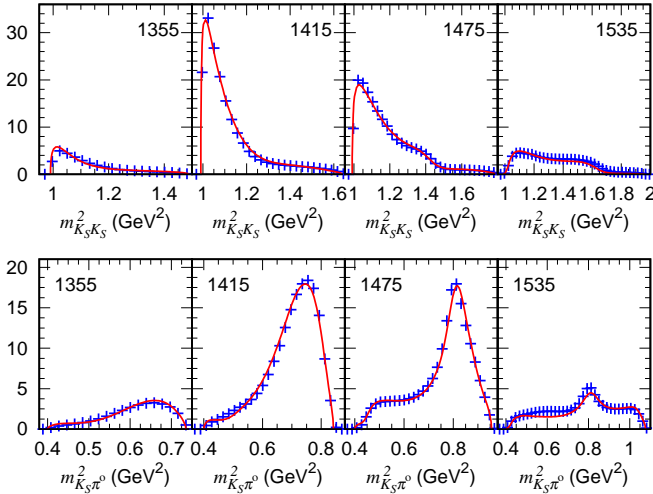


FIG. 2. The $K_S K_S$ (upper panels) and $K_S \pi^0$ (lower) invariant mass distributions. Our fit result (red solid curve) and the MC output (blue points) are shown. The E values (MeV) used in our calculation (the central values of the E bins of the MC) are indicated in each panel.

Results.— We fit the unitary coupled-channel model described above to experimental MC outputs, not to data directly, for radiative J/ψ decays. The BESIII MC for $J/\psi \rightarrow \gamma K_S K_S \pi^0$ [27] generates $K_S K_S \pi^0$ Dalitz plot distributions from its $J^{PC} = 0^{-+}$ partial wave amplitude (E -dependent solution) at each of 30 E bins (10 MeV bin width) in the range of $1300 \leq E \leq 1600$ MeV. Our coupled-channel model can be fitted to these Dalitz plot distributions that have been corrected for detection efficiency and background.

Our default model is also fitted simultaneously to ratios of partial decay widths, $R_1^{\text{exp}} = \Gamma[J/\psi \rightarrow \gamma \eta(1405/1475) \rightarrow \gamma(K \bar{K} \pi)] / \Gamma[J/\psi \rightarrow \gamma \eta(1405/1475) \rightarrow \gamma(\pi^+ \pi^- \eta)] \sim 6.8 - 11.9$ [14], and $R_2^{\text{exp}} = \Gamma[J/\psi \rightarrow \gamma \eta(1405/1475) \rightarrow \gamma(\rho^0 \gamma)] / \Gamma[J/\psi \rightarrow \gamma \eta(1405/1475) \rightarrow \gamma(K \bar{K} \pi)] = 0.015 - 0.043$ [12, 13]. We calculate the partial widths Γ by integrating the E distributions for the $K \bar{K} \pi$, $\pi^+ \pi^- \eta$, and $\pi^+ \pi^- \gamma$ final states over the range of $1350 \text{ MeV} < E < 1550 \text{ MeV}$. The above ratios can constrain parameters associated with the $f_0 \eta$ and $\rho \rho$ channels that are not well determined by the $K_S K_S \pi^0$ Dalitz plots. We obtained $R_1^{\text{th}} = 6.9$ and $R_2^{\text{th}} = 0.026$ after the fit.

The fits of a quite good quality are shown in Fig. 2 where the $a_0(980)$ and $K^*(892)$ peak structures in the $K_S K_S$ and $K_S \pi^0$ invariant mass distributions, respectively, are well reproduced⁵. The absolute values of the distributions are large in the $\eta(1405/1475)$ peak region

($E = 1.4 - 1.5 \text{ GeV}$). By integrating the distributions at each E , we obtain the E distribution shown in Fig. 3(a) by the red triangles. The E -distribution should reflect the pole structure of $\eta(1405/1475)$.

We show contributions from main $\eta^* \rightarrow K \bar{K} \pi$ decay mechanisms. The η^* decay mechanisms can be classified according to *final Rc* states in Fig. 1(a) that directly couple to the final *abc* states. As shown in Fig. 3(a), the final $K^* \bar{K}$ [magenta squares] and $\kappa \bar{K}$ [blue circles] give the first and second largest contributions, respectively. The clear $a_0(980)$ -like peak in the $K_S K_S$ invariant mass spectra (Fig. 2) is mostly formed by a constructive interference between the final $K^* \bar{K}$ and $\bar{K}^* K$ contributions at the $K_S K_S$ threshold; the small final $a_0(980) \pi$ contribution [green diamonds] slightly sharpens the peak through an interference.

Our decay mechanisms are rather different from the BESIII MC [27] where the $a_0(980) \pi$ contribution is the largest overall, and the $K^* \bar{K}$ contribution is comparable only at $E \sim 1500 \text{ MeV}$. There are three important improvements in our model: including the $\kappa \bar{K}$ channel, fitting the ratio R_1^{exp} , and accounting for the coupled-channel effects. The large R_1^{exp} is, albeit a large uncertainty, an important constraint on the final $a_0(980) \pi$ contribution to $K \bar{K} \pi$ since the coupling magnitude of $a_0(980) \rightarrow K \bar{K}$ relative to $a_0(980) \rightarrow \pi \eta$ is well determined experimentally [34]. Our $a_0(980) \pi$ contribution is small to fit R_1^{exp} , and the final $\kappa \bar{K}$ contribution is significant.

Among the coupled-channel mechanisms included in Fig. 1(a), direct decays [Fig. 1(b)] and single triangle mechanisms [Fig. 1(c)] play an important role. The direct-decay (single-triangle mechanism) is significantly larger in the final $K^* \bar{K}$ ($\kappa \bar{K}$ and $a_0(980) \pi$) contribution.

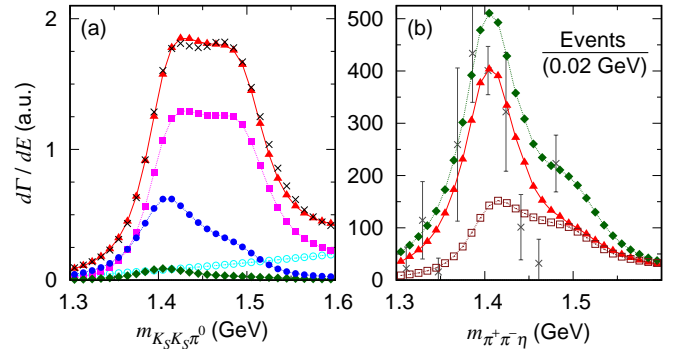


FIG. 3. The E distributions for $J/\psi \rightarrow \gamma \eta(1405/1475) \rightarrow \gamma(K_S K_S \pi^0)$ and (b) $\gamma(\pi^+ \pi^- \eta)$. The MC outputs [black crosses] of [27] and [7] are shown in (a) and (b), respectively. The red triangles are from the full calculation. Contributions are from the final $K^* \bar{K}$ ($\bar{K}^* K$) K_S [magenta squares] $\kappa \bar{K}$ ($\bar{\kappa} K$) K_S [blue circles], $a_0(980) \pi$ [green diamonds], and $f_0 \eta$ [brown open squares] states. The cyan circles are from a nonresonant amplitude. Lines connecting the points are just for guiding eyes.

⁵ The $K_S K_S \pi^0$ Dalitz plot distributions are shown in the Supplemental Material.

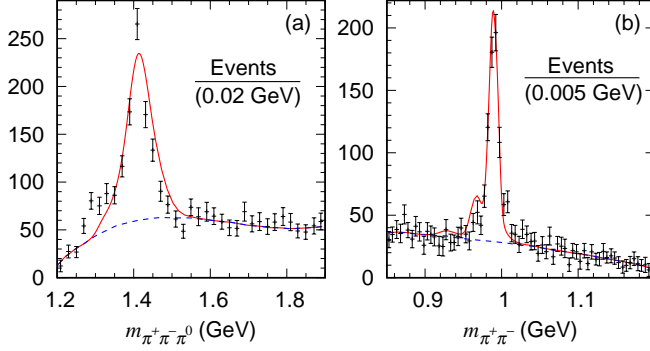


FIG. 4. Comparison with the BESIII data [29] for $J/\psi \rightarrow \gamma(\pi^+\pi^-\pi^0)$; (a) the $m_{\pi^+\pi^-\pi^0}$ and (b) $m_{\pi^+\pi^-}$ distributions. The blue dashed lines are the background polynomials from Ref. [29]. The red curve is from our full model, smeared with the bin width, scaled to fit the data, and augmented by the background.

Figure 3(a) shows that the broad peak structure from the full calculation is mainly formed by the final $K^*\bar{K}$ contribution.

To address the question whether $\eta(1405/1475)$ is one or two states, we also attempted to fit the BESIII MC output for $K_S K_S \pi^0$ with a single bare η^* model. The final $\kappa\bar{K}$ and $a_0\pi$ contributions have similar lineshapes peaking at $E \sim 1420$ MeV, while the final $K^*\bar{K}$ contribution has a peak at 30–40 MeV higher since $K^*\bar{K}$ is relatively p -wave and its threshold is at $E \sim 1400$ MeV. Their coherent sum cannot reproduce the ~ 100 MeV wide flat peak, even if fitting the E distribution only. We thus conclude that two bare η^* states are necessary to explain the BESIII MC’s 0^{-+} contribution.

Now our default model makes predictions for $\eta^* \rightarrow \pi\pi\pi$ and $\pi\pi\eta$. The predicted E dependence for $J/\psi \rightarrow \gamma\eta(1405/1475) \rightarrow \gamma(\eta\pi^+\pi^-)$ is shown in Fig. 3(b). The lineshape is consistent with the MC [7, 8]. Although both $K\bar{K}\pi$ and $\pi\pi\eta$ originate from the same η^* resonances, the $\pi\pi\eta$ final states give a single peak at $m_{\pi\pi\eta} \sim 1400$ MeV while the $m_{K\bar{K}\pi}$ distribution has the broad peak. This is because $K\bar{K}\pi$ and $\pi\pi\eta$ are from different final Rc states that have different E dependences. As shown in Fig. 3(b) the final $a_0(980)\pi$ contribution [green diamonds] mostly explains the full result [red triangles] for the $\pi\pi\eta$ final states. The final $f_0\eta$ contribution is significantly smaller. On the other hand, the $K\bar{K}\pi$ final states are mainly from the final $K^*\bar{K}$ and $\kappa\bar{K}$ contributions, as seen in Fig. 3(a). This is a natural explanation why the $\eta(1405/1475)$ lineshapes are different in different final states.

For the isospin-violating $J/\psi \rightarrow \gamma\eta(1405/1475) \rightarrow \gamma(\pi\pi\pi)$, our coupled-channel model predicts the $m_{\pi^+\pi^-\pi^0}$ and $m_{\pi^+\pi^-}$ distributions as shown in Fig. 4(a) and 4(b), respectively, in good agreement with the BESIII data [29]. The authors of Refs. [23, 24, 26] pro-

posed that these processes are dominantly caused by the $K^*K\bar{K}$ triangle loop mechanisms [Fig. 1(c)]. While the $K^*K^+K^-$ and $K^*K^0\bar{K}^0$ triangle loops cancel with each other almost exactly for the isospin symmetry, due to $m_{K^\pm} \neq m_{K^0}$, a significant isospin violation occurs in the small window of $2m_{K^\pm} \lesssim m_{\pi^+\pi^-} \lesssim 2m_{K^0}$. The mechanism satisfies the kinematical condition to cause a triangle singularity at $m_{\pi^+\pi^-\pi^0} \sim 1410$ MeV and $m_{\pi^+\pi^-} \sim 2m_K$, and the peaks appear as a result as shown in Fig. 4. This mechanism is required by the three-body unitarity and, thus, automatically included in our calculation.

The $K\bar{K}\pi$ and $\pi\pi\pi$ branching ratios in Refs. [14, 29] give ratios: $\Gamma[J/\psi \rightarrow \gamma\eta(1405/1475) \rightarrow \gamma(\pi^+\pi^-\pi^0)] / \Gamma[J/\psi \rightarrow \gamma\eta(1405/1475) \rightarrow \gamma(K\bar{K}\pi)] \sim 0.004 - 0.007$ and $\Gamma[J/\psi \rightarrow \gamma\eta(1405/1475) \rightarrow \gamma(\pi^0\pi^0\pi^0)] / \Gamma[J/\psi \rightarrow \gamma\eta(1405/1475) \rightarrow \gamma(K\bar{K}\pi)] \sim 0.002 - 0.003$. Our coupled-channel model predicts 0.0049 and 0.0016, respectively, in good agreement with the experimental ones. These reasonable predictions for the $\pi\pi\eta$ and $\pi\pi\pi$ final state would support the model’s dynamical contents determined by the fits.

Finally, we find η^* poles (E_{η^*}) that satisfy $\det[\bar{G}^{-1}(E_{\eta^*})] = 0$, with $\bar{G}^{-1}(E)$ in Eq. (4), by analytically continuing the amplitude [35, 36]. Three poles labeled by $\alpha = 1, 2$ [$\alpha = 3$] correspond to $\eta(1405)$ [$\eta(1475)$] as shown in Table I. The mass and width values are fairly similar to the BESIII result (BW parameters) also shown in the table. The poles are close to the branch points associated with the $K^*(892)\bar{K}$ and $a_2(1320)\pi$ channels as shown in Fig. 5. Thus we specify the Riemann sheet (RS) of these channels in Table I⁶. The two-pole structure of $\eta(1405)$ in our model does not mean two physical states but is simply due to a general fact that a pole is split into two poles on different RS of its decay channel; when the pole is located near the channel threshold, both poles on different RS can be close to the physical

TABLE I. Pole locations; the unit is MeV. Poles are labeled by $\alpha = 1, 2$, and 3. The mass (M) and width (Γ) are $M = \text{Re}[E_{\eta^*}]$ and $\Gamma = -2\text{Im}[E_{\eta^*}]$ where E_{η^*} is a pole position. The Riemann sheets (RS) of the pole positions are specified by $(s_{K^*\bar{K}}, s_{a_2(1320)\pi})$ where $s_x = p(u)$ indicates that a pole is on the physical (unphysical) sheet of the channel x . The BW masses and widths from the BESIII analysis are also shown.

	$\alpha = 1$	$\alpha = 2$	$\alpha = 3$	BESIII [27]	
M	1392	1404	1502	1391.7 ± 0.7	1507.6 ± 1.6
Γ	76	74	90	60.8 ± 1.2	115.8 ± 2.4
RS	(pp)	(up)	(up)		

⁶ Section 50 “Resonances” in Ref. [14] defines the (un)physical sheet.

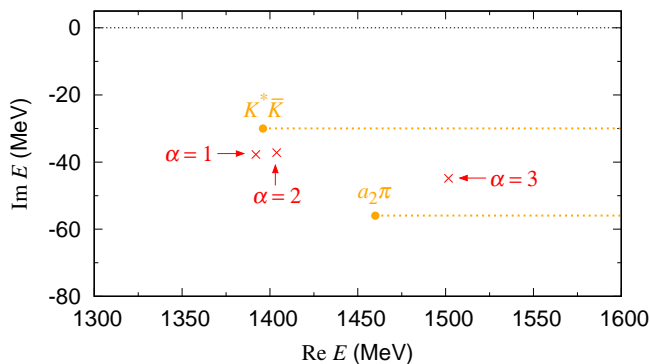


FIG. 5. Locations of the $\alpha = 1, 2, 3$ poles in Table I. The orange circles are the $K^*(892)\bar{K}$ and $a_2(1320)\pi$ branch points, and the dotted horizontal lines are the branch cuts.

real energies and thus relevant. As a consequence of the unitarity, the pole structure (η^* propagation) and the Dalitz plot distributions (η^* decay mechanism) are connected by the common dynamics in our model but not in the BW model.

The bare states in our model are conceptually similar to states given by quark models or LQCD without two-hadron operators. The new BESIII data [27] require two bare states. The lighter one of ~ 1.6 GeV seems to be compatible with the excited $s\bar{s}$ [14, 15]. The heavier bare mass can be in the range of 2–2.4 GeV to give comparable fits. This state could be either of a second radial excitation of $\eta^{(\prime)}$, hybrid [16], glueball [18–22], or a mixture of those. The two bare states are mixed and dressed by continuum coupled-channels to form the $\eta(1405/1475)$ poles.

Summary and Outlook.— We conducted a coupled-channel analysis of radiative J/ψ decays via $\eta(1405/1475)$, and addressed the long-standing $\eta(1405/1475)$ puzzles itemized in the Introduction. Our three-body unitary coupled-channel model is reasonably fitted to the $K_S K_S \pi^0$ Dalitz plot distributions generated by the BESIII’s partial wave amplitudes [27], and also to branching fractions of $\eta\pi^+\pi^-$ and $\gamma\pi^+\pi^-$ final states relative to that of $K\bar{K}\pi$. The model predicts the different $\eta(1405/1475)$ lineshapes for the $\eta\pi^+\pi^-$ and $\pi\pi\pi$ final states in reasonable agreement with experimental results. The model also well predicts the branching fractions for the isospin-violating $\pi\pi\pi$ final states and their narrow $f_0(980)$ -like $\pi^+\pi^-$ lineshape; the triangle singularity effect automatically included in our unitary model plays a crucial role. Our model revealed the $\eta(1405/1475)$ pole structures for the first time. Two poles on different Riemann sheets of the $K^*\bar{K}$ channel correspond to $\eta(1405)$, and one pole for $\eta(1475)$.

We emphasize that most of the present analysis results heavily depend on the experimentally determined 0^{-+} contributions to the radiative J/ψ decays [7, 8, 12, 13,

27]. In future, the presented analysis for 0^{-+} should be extended to include more J^{PC} to analyze the radiative J/ψ decay data directly, addressing pole structures of $\eta(1405/1475)$, $f_1(1420)$, etc. with the unitary coupled-channel framework consistently.

The authors thank the BESIII Collaboration for providing us with the MC outputs for our study. The authors also thank T.-S. Harry Lee, Bei-Jiang Liu, Xiao-Hai Liu, Guo-Fa Xu, Qiang Zhao, and Bing-Song Zou for useful discussions. This work is in part supported by National Natural Science Foundation of China (NSFC) under Grants No.U2032103, U2032111, 11625523, 12175239, 12221005, and also by National Key Research and Development Program of China under Contracts 2020YFA0406400.

Supplemental material

* satoshi@ustc.edu.cn

† wujiajun@ucas.ac.cn

- [1] G.S. Adams et al. (E852 Collaboration), Observation of Pseudoscalar and Axial Vector Resonances in $\pi^- p \rightarrow K^+ K^- \pi^0 n$ at 18 GeV, Phys. Lett. B **516**, 264 (2001).
- [2] M.G. Rath et al., The $K_S^0 K_S^0 \pi^0$ system produced in $\pi^- p$ interactions at 21.4 GeV/c, Phys. Rev. D **40**, 693 (1989).
- [3] F. Nichitiet et al. (OBELIX Collaboration), Study of the $K^+ K^- \pi^+ \pi^- \pi^0$ final state in antiproton annihilation at rest in gaseous hydrogen at NTP with the OBELIX spectrometer, Phys. Lett. B **545**, 261 (2002).
- [4] Z. Bai et al. (MARKIII Collaboration), Partial-wave analysis of $J/\psi \rightarrow \gamma K_S^0 K^\pm \pi^\mp$, Phys. Rev. Lett. **65**, 2507 (1990).
- [5] J.-E. Augustin et al. (DM2 Collaboration), Partial-wave analysis of DM2 Collaboration data in the $\eta(1430)$ energy range, Phys. Rev. D **46**, 1951 (1992).
- [6] C. Amsler et al., Production and decay of $\eta'(958)$ and $\eta(1440)$ in $p\bar{p}$ annihilation at rest, Eur. Phys. J. C **33**, 23 (2004).
- [7] T. Bolton et al., Partial-wave analysis of $J/\psi \rightarrow \gamma\eta\pi^+\pi^-$, Phys. Rev. Lett. **69**, 1328 (1992).
- [8] J.-Z. Bai et al. (BES Collaboration), Partial wave analysis of $J/\psi \rightarrow \gamma(\eta\pi^+\pi^-)$, Phys. Lett. B **446**, 356 (1999).
- [9] J.-E. Augustin et al. (DM2 Collaboration), Radiative decay of J/ψ into $\eta(1430)$ and nearby states, Phys. Rev. D **42**, 10 (1990).
- [10] M. Ablikim et al. (BESIII Collaboration), $\eta\pi^+\pi^-$ Resonant Structure around 1.8 GeV/ c^2 and $\eta(1405)$ in $J/\psi \rightarrow \omega\eta\pi^+\pi^-$, Phys. Rev. Lett. **107**, 182001 (2011).
- [11] M. Acciarri et al. (L3 Collaboration), Light resonances in $K_S^0 K^\pm \pi^\mp$ and $\eta\pi^+\pi^-$ final states in $\gamma\gamma$ collisions at LEP, Phys. Lett. B **501**, 1 (2001).
- [12] J.Z. Bai et al. (BES Collaboration), A Study of $J/\psi \rightarrow \gamma\gamma V(\rho, \phi)$ decays with the BESII detector, Phys. Lett. B **594**, 47 (2004).

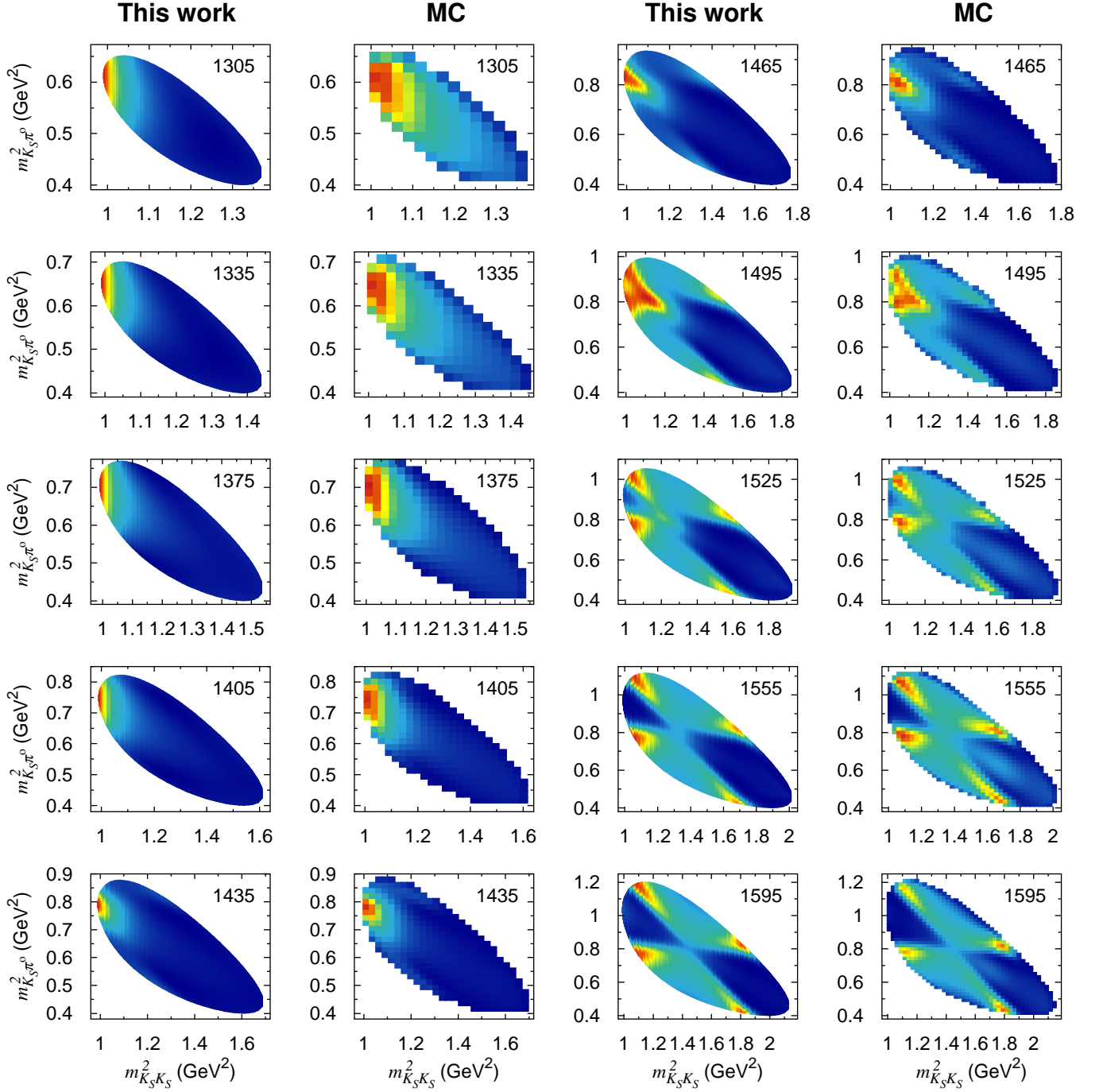


FIG. 6. The $K_S K_S \pi^0$ Dalitz plot distribution in $J/\psi \rightarrow \gamma \eta(1405/1475) \rightarrow \gamma(K_S K_S \pi^0)$. The $K_S K_S \pi^0$ invariant mass (MeV) is indicated in each panel.

- [13] D. Coffman et al. (MARK-III Collaboration), Study of the doubly radiative decay $J/\psi \rightarrow \gamma \gamma \rho^0$, Phys. Rev. D **41**, 1410 (1990).
- [14] P.A. Zyla et al. (Particle Data Group), The Review of Particle Physics, Prog. Theor. Exp. Phys. **2020**, 083C01 (2020).
- [15] T. Barnes, F. E. Close, P. R. Page, and E. S. Swanson, Higher quarkonia, Phys. Rev. D **55**, 4157 (1997).
- [16] J.J. Dudek, R.G. Edwards, P. Guo, and C.E. Thomas, (Hadron Spectrum Collaboration), Toward the excited isoscalar meson spectrum from lattice QCD, Phys. Rev. D **88**, 094505 (2013).
- [17] L. Faddeev, A.J. Niemi and U. Wiedner, Glueballs, closed fluxtubes, and $\eta(1440)$, Phys. Rev.D **70**, 114033 (2004).
- [18] G.S. Bali, K. Schilling, A. Hulsebos, A.C. Irving, C. Michael, and P.W. Stephenson (UKQCD Collaboration),

- A comprehensive lattice study of SU(3) glueball, Phys. Lett. B **309**, 378 (1993).
- [19] C.J. Morningstar and M.J. Peardon, Glueball spectrum from an anisotropic lattice study, Phys. Rev. D **60**, 034509 (1999).
 - [20] Y. Chen, A. Alexandru, S.J. Dong, T. Draper, I. Horvath, F.X. Lee, K.F. Liu, N. Mathur et al., Glueball spectrum and matrix elements on anisotropic lattices, Phys. Rev. D **73**, 014516 (2006).
 - [21] C.M. Richards, A.C. Irving, E.B. Gregory, and C. McNeile (UKQCD Collaboration), Glueball mass measurements from improved staggered fermion simulations, Phys. Rev. D **82**, 034501 (2010).
 - [22] F. Chen, X. Jiang, Y. Chen, K.-F. Liu, W. Sun, and Y.-B. Yang, Glueballs at Physical Pion Mass, arXiv:2111.11929 [hep-lat].
 - [23] J.-J. Wu, X.-H. Liu, Q. Zhao, and B.-S. Zou, Puzzle of Anomalously Large Isospin Violations in $\eta(1405/1475) \rightarrow 3\pi$ in the J/ψ radiative decay, Phys. Rev. Lett. **108**, 081803 (2012).
 - [24] X.-G. Wu, J.-J. Wu, Q. Zhao, and B.-S. Zou, Understanding the property of $\eta(1405/1475)$ in the J/ψ radiative decay, Phys. Rev. D **87**, 014023 (2013).
 - [25] F. Aceti, W. H. Liang, E. Oset, J. J. Wu and B. S. Zou, Isospin breaking and $f_0(980)$ - $a_0(980)$ mixing in the $\eta(1405) \rightarrow \pi^0 f_0(980)$ reaction, Phys. Rev. D **86**, 114007 (2012).
 - [26] M.-C. Du and Q. Zhao, Internal particle width effects on the triangle singularity mechanism in the study of the $\eta(1405)$ and $\eta(1475)$ puzzle, Phys. Rev. D **100**, 036005 (2019).
 - [27] M. Ablikim et al. (BESIII Collaboration), Study of $\eta(1405)/\eta(1475)$ in $J/\psi \rightarrow \gamma K_S^0 K_S^0 \pi^0$ decay, arXiv:2209.11175 [hep-ex].
 - [28] S.X. Nakamura, H. Kamano, T.-S.H. Lee, T. Sato, Extraction of meson resonances from three-pions photo-production reactions, Phys. Rev. D **86**, 114012 (2012).
 - [29] M. Ablikim et al. (BESIII Collaboration), First Observation of $\eta(1405)$ Decays into $f_0(980)\pi^0$, Phys. Rev. Lett. **108**, 182001 (2012).
 - [30] S.X. Nakamura, Q. Huang, J.-J. Wu, H.P. Peng, Y. Zhang, and Y.C. Zhu, in preparation.
 - [31] H. Kamano, S.X. Nakamura, T.-S.H. Lee, and T. Sato, Unitary coupled-channels model for three-mesons decays of heavy mesons, Phys. Rev. D **84**, 114019 (2011).
 - [32] M. Bando, T. Kugo, and K. Yamawaki, Nonlinear realization and hidden local symmetries, Phys. Rept. **164**, 217 (1988).
 - [33] S.X. Nakamura, Coupled-channel analysis of $D^+ \rightarrow K^- \pi^+ \pi^+$ decay, Phys. Rev. D **93**, 014005 (2016).
 - [34] A. Abele et al., $\bar{p}p$ annihilation at rest into $K_L K^\pm \pi^\mp$ Phys. Rev. D **57**, 3860 (1998).
 - [35] N. Suzuki, T. Sato, and T.-S.H. Lee, Extraction of resonances from meson-nucleon reactions, Phys. Rev. C **79**, 025205 (2009).
 - [36] W. Glöckle, S-matrix pole trajectory in a three-neutron model, Phys. Rev. C **18**, 564 (1978).